

GIS-Aided Propagation Prediction Study for Broadcast and Telecommunication Services

A. Altintas, I. Aksun, O. Balta, H. Koymen, S. Topcu, and V. Yurchenko^{†*},

Electrical and Electronics Engineering Department, Bilkent University

Bilkent, 06533 Ankara, Turkey

Phone: +90-312-290-1489 Fax: +90-312-266-4307 E-mail: *altintas@ee.bilkent.edu.tr*[†]

Experimental Physics Department, National University of Ireland

Maynooth, Co. Kildare, Ireland

Phone: +353-1-708-3746 Fax: +353-1-708-3313 E-mail: *v.yurchenko@may.ie*^{*}

Institute of Radiophysics and Electronics, National Academy of Sciences of Ukraine

12 Proskura St., Kharkov, 61085, Ukraine

Phone: +38-0572-44-8349 Fax: +38-0572-44-1105 E-mail: *yurchenk@ire.kharkov.ua*

1. Introduction

The aim of this work was to develop a propagation simulation software which implements various methods for predicting broad-band propagation characteristics covering both broadcast and telecommunication services. This software is integrated with a Geographic Information System (GIS) and covers any type of terrain profiles, ranging from smooth and planar earth profile to irregular inhomogeneous mountainous terrain, so that various propagation prediction models can be compared with each other and with the parabolic wave equation solution on a real terrain profile.

The implemented methods employed here cover most of the frequency bands being currently in use for both TV and radio broadcast, for mobile communications, and for special telecommunication services, from VLF to UHF and higher frequencies. Standard prediction methods recommended by International Telecommunications Union (ITU) and some others given in the literature have been implemented and compared for their accuracies and applicabilities.

2. Propagation models according to ITU Recommendations

Propagation prediction schemes include CCIR curves with Δh , clearance angle, mixed path corrections and other suggested modifications for VHF–UHF bands [1]. In addition, multiple diffraction is accounted for by following the ITU recommendation 526 [2] and by

Epstein-Peterson, Deygout or Vogler methods [3-6]. For urban areas and higher frequencies, Okumura-Hata, ITU Recommendation 1146 or Walfish-Ikegami models are implemented [7-12]. For lower frequencies, standard programs developed and distributed by ITU are utilized. System is flexible and allows to include any other available methods, modules or software.

Because of complicated mountainous landscape typical for Turkey, a special study has been performed to compare the predictions of different methods when applied to real terrain. Figure 1 shows a real terrain profile away from the transmitter site 'A' which has an effective radiated power of 1 kW at $f = 30\text{MHz}$. The terrain data is in the DTED Level 1 format which has a resolution of 3 by 3 arcseconds.

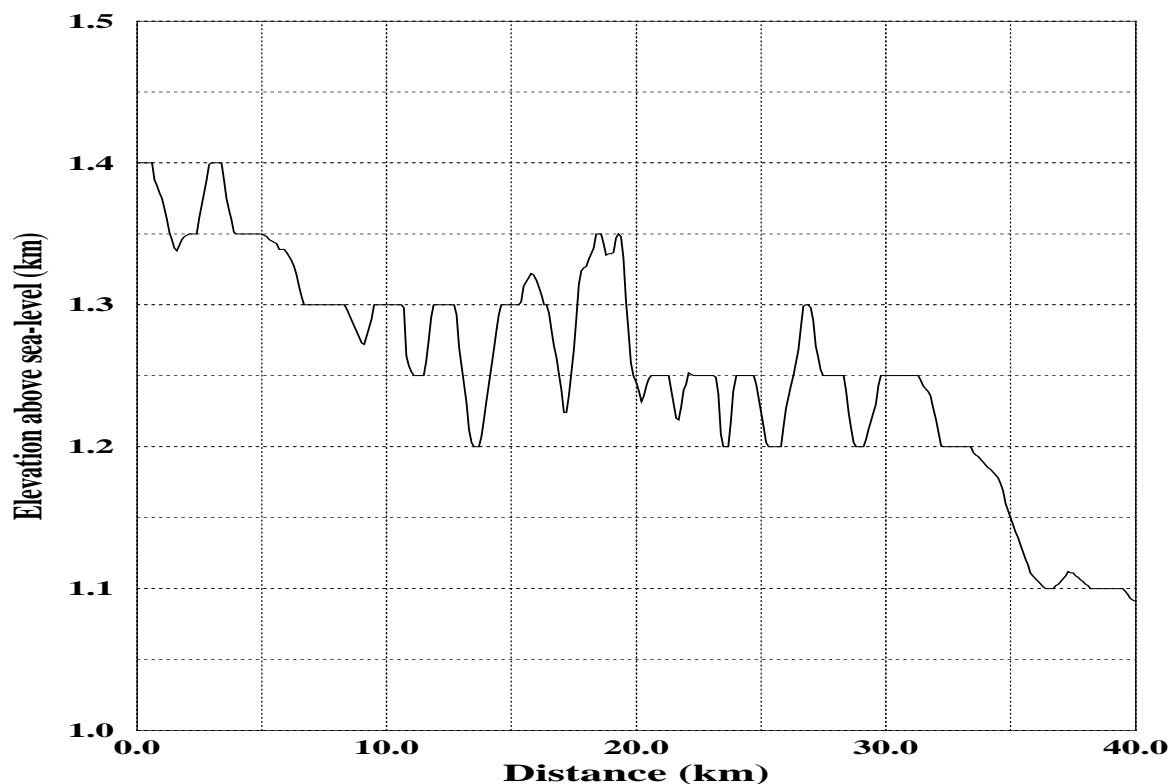


Fig. 1. Terrain profile above sea-level from TX-site 'A' (N 39° 30' 30", E 32° 37' 45") in the 180° azimuthal direction.

Particular attention has been paid to various methods available for VHF-UHF and higher bands (Figures 2 and 3). As seen in Figure 2, CCIR curves yield generally higher field strength predictions. Although inclusion of Δh correction improves this, it is not to a satisfactory level because of neglecting the shadowing immediately after the hilltops, which can be accounted for by the inclusion of clearance angle correction. Multiple diffraction models such as Epstein-Peterson, Deygout or Vogler are intended for the better prediction of diffraction loss. Shadowing effect is similarly predicted by all of the diffraction models, but

they differ more in the average signal level, as shown in Figure 2. Note that Epstein-Peterson method predicts on the high side and the Vogler method does on the low side in terms of the average signal level. However, simplicity in applying the Epstein-Peterson method may make it more favorable for some applications.

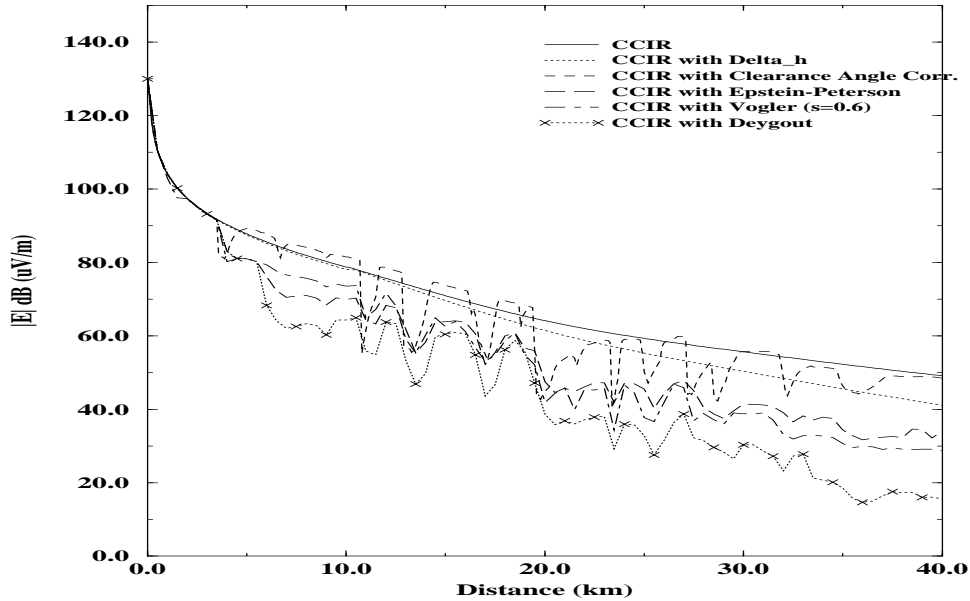


Fig. 2. Comparison of the field strengths predicted by different corrections to CCIR.

It is noted that the Vogler method does not specify how to choose significant knife-edges for simulations when the terrain data are available in the form of the elevation database. To solve the problem, an original selection procedure has been developed which accounts for both the distance and the depth of the valleys between local terrain maxima considered as potential knife-edges for being accounted in simulations. Since accounting for too many maxima grossly overestimate the losses, a flexible selection criterion has been introduced. The selection parameter s is the fraction of the Fresnel zone used for making the decision whether two adjacent local maxima to be accounted either as two different knife-edges separated by significant valley or as a single dominating knife-edge representing an extended hill. The decision is made by the rule that two maxima are distinguished if there is a point in the valley located outside the fraction s of the Fresnel zone connecting the maxima. Alternatively, the maxima are not distinguished if the whole valley is located inside the given fraction of the Fresnel zone. The comparison of the field strength values using different s values is shown in Figure 3. Note that $s = 0$ is the case when all the local peaks are accounted for as different knife-edges. As seen, this yields lowest values of the field strength. For practical purposes, $s = 0.6$ seems to be satisfactory.

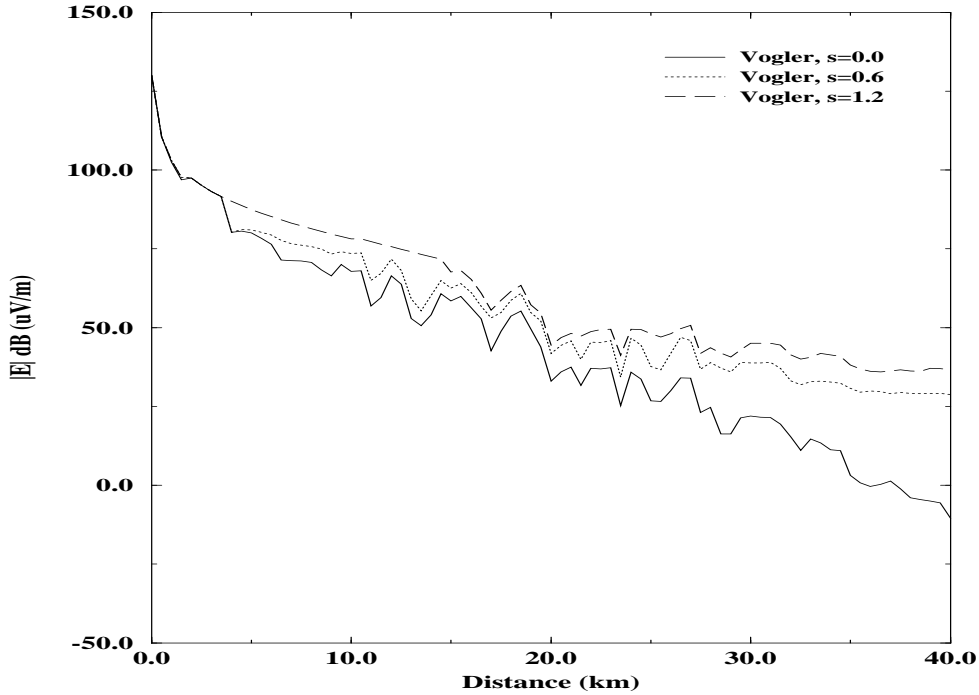


Fig. 3. Comparison of the field strengths predicted by the Vogler method with different selection parameter s .

3. Propagation by parabolic wave equation

Another issue of our research has been a comparison of the knife-edge diffraction models with the parabolic wave equation approximation. The comparison is of importance for both proper selection of significant maxima for multiple-edge diffraction models and for studying the effect of the terrain between the selected knife-edges for such models.

Propagation model based on the parabolic wave equation (PWE) is a powerful theoretical method for studying tropospheric radiowave propagation over irregular terrain. The importance of the PWE model relies on its capability to properly estimate the combined effects of the wave reflection from the ground, refraction in the troposphere and diffraction by complicated landscape features.

In our analysis, we use the finite-difference approach utilizing Crank-Nicholson algorithm [13] for solving two-dimensional version of the PWE. The main advantage of the Crank-Nicholson method is that it provides stability, efficiency and second-order accuracy of the solution in terms of mesh increments in both variables, while conserving the total power of the propagating wave.

3.1. PWE approximation

We consider two-dimensional parabolic equation in cylindrical coordinates, obtained from the Helmholtz wave equation by assuming slowly varying amplitude and axial symmetry of

propagating wave. Using the substitution

$$\Psi(r, z) = A(x, \eta) \exp(ix)/\sqrt{x} \quad (1)$$

where $\Psi(r, z)$ is either E_z or E_ϕ component of the wave electric field in the case of either vertical or horizontal polarization, respectively, $x = kr$, $\eta = kz$, and k is the wavenumber, we obtain the parabolic wave equation in the form

$$\frac{\partial^2 A}{\partial \eta^2} + 2i \frac{\partial A}{\partial x} + \frac{1}{4x^2} A = 0 \quad (2)$$

where the term $A/(4x^2)$ is vanishing when $x \gg 1$.

The main restrictions of the PWE approximation are that Eq.(2) neglects back-scattered field, polarization effects, large-angle propagation with respect to horizon, and diffusive scattering due to the rough surface, although various improvements and modifications [14-16] help to relax these restrictions. The advantage of the method is that Eq.(2) can be solved by rather simple and efficient forward marching along the propagation direction x .

3.2. Computational domain and boundary conditions

Equation (2) has to be solved in the domain $x_{min} < x < x_{max}$ and $\eta_h(x) < \eta < \eta_{max}$ where x_{min} and x_{max} define the range of propagation, $\eta_h(x) = kh(x)$ is the bottom boundary function, $h(x) = H(r) - H(r_T) - r^2/R$, $H(r)$ is the terrain elevation above sea level, $H(r_T)$ is the transmitter ground level, r_T is the position of the transmitter, R is the effective Earth radius (thus, the function $h(x)$ accounts for both the Earth curvature and the atmospheric refraction), and η_{max} is the top boundary needed to restrict the computational domain.

Boundary conditions are formulated at the initial vertical boundary $x = x_{min}$ where the source field distribution $A(x_{min}, \eta) = A_0(\eta)$ has to be given. Boundary conditions at the top and bottom boundaries, ($\eta = \eta_{max}$ and $\eta = \eta_h(x)$, respectively) have to be imposed as described below.

3.2.1. Conditions at the top boundary

At the top boundary, we should impose some discrete form of a non-reflective boundary condition. The particular formulation depends on the method of solution and on the implementation. Some forms are inadequate, despite their use in publications. For example, the explicit form of non-radiative condition used in [14] means merely that the energy flux through the top boundary $\eta = \eta_{max}$ is just the same constant at any propagation distance x as it was at the initial position $x = x_{min}$. Implicit forms of such a condition eliminate this restriction but, instead, they introduce instability in computation that appears, as we observed, in the case of complicated terrain profile and, especially, with increasing the order of approximation in the discrete form of the condition.

More appropriate forms of the top boundary condition are the absorbing boundary condition and apodization. In our simulations, we used a simple form of apodization by a quarter period of a sinusoid decaying from one to zero at the top layer of the width about $0.3\eta_{max}$ where η_{max} varied, in most cases, from about $1km$ up to $4km$ (in special trials) while the wavelength was $\lambda = 10m$ (frequency $f = 30MHz$). Note that η_{max} has to be consistent with the requirement $z_{max}^2 > \lambda r_{max}$ that, in the cases mentioned above, allows to get distances about $r_{max} \approx 100km$.

3.2.2. Boundary conditions at the ground

Boundary conditions at the Earth surface depend on the ground conductivity and on the polarization of electromagnetic wave. In the case of dielectric ground of low conductivity, we should consider wave penetration into the ground and choose η_{min} below $\min(\eta_h(x))$. In our case, we imposed standard continuity boundary conditions on electric and magnetic fields at the air-ground interface $\eta = \eta_h(x)$ and used apodization at η_{min} similar to η_{max} . However, numerical solutions in the case of dielectric ground for the real complicated terrain were rather unstable and unreliable in both vertical and horizontal polarizations considered.

Due to large values of the relative dielectric constant ϵ_r , as well as in the case of rather conductive ground, we can apply the impedance boundary condition at the ground surface. This approximation appeared to be the most practical one to account for the ground properties. Application of the discrete form of the impedance boundary condition to non-smooth irregular terrain is, however, rather complicated matter. Generally, it requires non-uniform mesh in x direction that depends on the terrain slope at any given point x . For mountainous terrain with very steep slopes, it is not very practical.

Trials of different forms of discrete boundary condition that account for the value of slope and include extra vertical nodes to preserve a uniform mesh in x direction did not improve solution as well. Generally, in the mountainous region at the distances exceeding a few dozens kilometers, the solution is getting unstable and unreliable, even though it works well for smooth surfaces.

The simplest form of the ground boundary condition is realized in the approximation of the perfect electrical conductor (PEC) ground. For the horizontal polarization, we obtain

$$\Psi|_{\eta=\eta_h(x)} = 0, \quad (3)$$

while for the vertical polarization

$$\partial\Psi/\partial\tau|_{\eta=\eta_h(x)} = 0 \quad (4)$$

where τ is the tangent coordinate along the surface. Notice that treating polarization of a non-uniform electromagnetic wave by the scalar equation (2) is approximate in both cases, rather than in the case of vertical polarization alone as stated in [15].

In PEC approximation, straightforward implementation of the boundary condition (3) results in a stable solutions for rather long distances while more complicated condition (4) exhibits the same problems as the impedance boundary condition discussed above.

The best solution to the problem has been achieved by means of an appropriate transformation of the computational domain that reduces the complicated shape of the air-ground interface to the straight line as proposed in [17]. With the substitution

$$\zeta = \eta - \eta_h(x), \quad (5)$$

the complex amplitude function $A(x, \eta)$ can be presented as

$$A(x, \eta) = U(x, \zeta) \exp[i\Theta(x, \zeta)] \quad (6)$$

where

$$\Theta(x, \zeta) = \zeta \eta'_h(x) + \frac{1}{2} \int_{x_{min}}^x (\eta'_h(x))^2 dx \quad (7)$$

(similar function in [17] contains mistyped coefficient 3/2 instead of correct 1/2), and $U(x, \zeta)$ satisfies another parabolic equation

$$\frac{\partial^2 U}{\partial \zeta^2} + 2i \frac{\partial U}{\partial x} + V(x, \zeta)U = 0 \quad (8)$$

with

$$V(x, \zeta) = \zeta \eta''_h(x) - 1/(8x^2). \quad (9)$$

The impedance boundary condition takes the form

$$\left(\partial U / \partial \zeta + [\alpha + \eta'_h(x)] U \right) |_{\zeta=0} = 0 \quad (10)$$

where $\alpha = ikn_c$ for the horizontal polarization, $\alpha = ik/n_c$ for the vertical one, and $n_c = (\epsilon_r + i\sigma/(2\pi f\epsilon_0))^{1/2}$.

In the PEC approximation, it is reduced to $U|_{\zeta=0} = 0$ and $(\partial U / \partial \zeta + \eta'_h(x) U) |_{\zeta=0} = 0$ for horizontal and vertical polarization, respectively. Thus, the transformation reduces the problem of formulating boundary conditions at the boundary of complicated shape to the problem with a simple boundary but involving, instead, the task of computing the first and second derivatives of irregular terrain elevation function.

Such a transformation illustrates the nature of difficulties in the problem: generally, the inner corners of a complicated domain result in local singularities of a solution while numerical evaluation of derivatives, especially of a higher order, is a typical ill-posed problem that results in numerical instability (also, the derivatives are not unique at the corners).

Nevertheless, conformal mapping described above helps to facilitate the problem since various regularized approaches can be used for numerical evaluation of derivatives that makes the problem much more robust.

In our simulations, we have used standard cubic spline interpolation of the terrain elevation data in order to get reasonably simple and stable numerical evaluation of derivatives. Although the second derivative is not getting smooth by this approach, it is continuous and perfectly stable that was sufficient for solving equation(8) with quite complicated terrain for rather long distances in both horizontal and vertical polarizations.

The results of our PWE simulations are shown in Figure 4 for both polarizations. For comparison, CCIR curves and the diffraction loss based on the Vogler method are also shown in the figure. Horizontal polarization case agrees generally with the Vogler method. Naturally in the PWE solution, the size of the window height has to be chosen suitably. The effect of the window height on the results is shown in Figure 5.

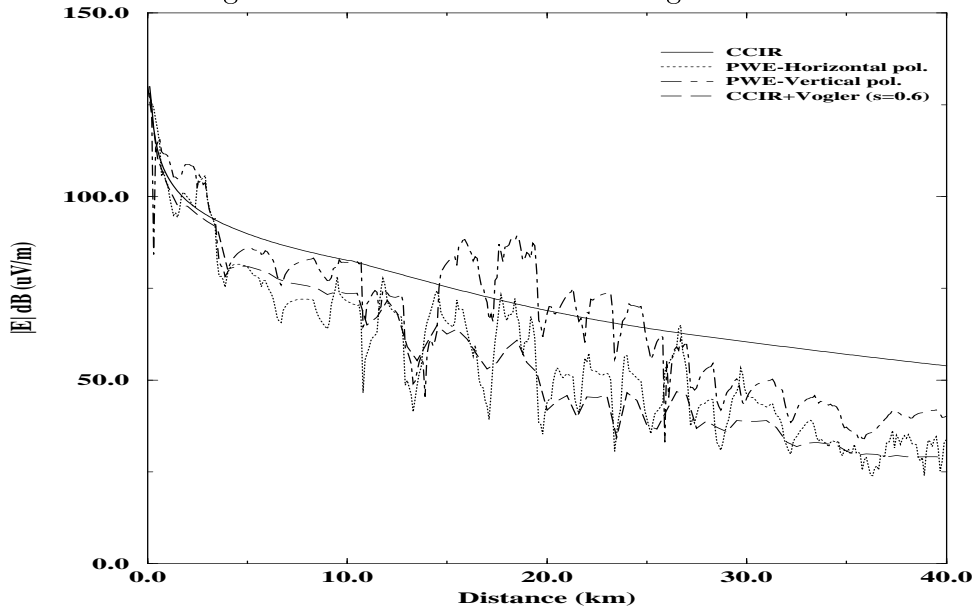


Fig. 4. Comparison of PWE solutions with CCIR and Vogler methods.

3.3. Source of radiation

In all the publications cited above, PWE approximation has been used for propagating smooth initial field distribution given at the vertical boundary $x = x_{min}$. Typically, it is a Gaussian beam approximating the main lobe of the far-field pattern of a radar. The source

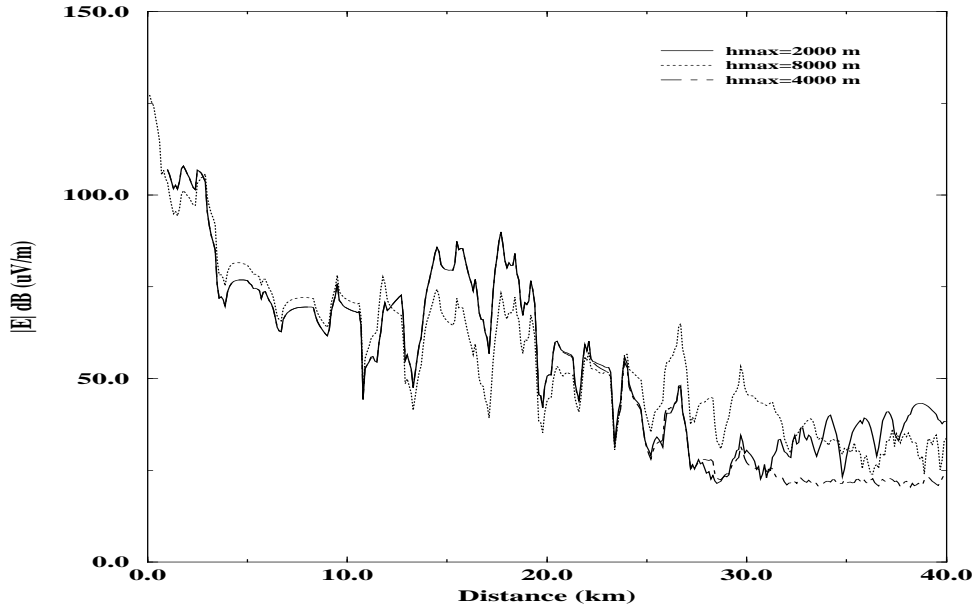


Fig. 5. Comparison of PWE solutions for different computation window heights.

field in conventional broadcast and telecommunication problems is, however, qualitatively different. The transmitter is generally considered as a point source radiating as an electric dipole, sometime with an additional pattern providing some angular power distribution.

Although the dipole model is simple and the power pattern is smooth, phase variations at the distant vertical planes are quite rapid that requires a fine mesh in vertical coordinate ζ and, as a result, at least the same fine mesh in propagation direction x . In practice, we used a few nodes per wavelength in both directions, taking into account that overall stability and reliability of solutions obtained by the Crank-Nicholson method were much better when both increments in ζ and x were comparable.

In order to obtain the initial field at the boundary $x = x_{min}$, we assumed the horizontal or vertical electric dipole antenna located at the height h_T above the PEC plane extended from the ground level at the transmitter site ($\eta_h(x_T) = 0$) to the ground point at the initial boundary ($\eta = \eta_h(x_{min})$). The value of x_{min} typically varied from 30 to 300 that did not affect the results essentially. The field propagated from the antenna to the point x_{min} was evaluated as a field of the electric dipole radiating over the tilted PEC plane.

4. GIS Integration

As seen from the above discussions, large-scale field strength prediction models may yield substantially different results. The factors affecting the decision of which model to choose depend on the type of landscape, services and frequency band, but it may not be totally based on technical concerns. Some governmental regulatory bodies may prefer to impose one particular model. So, the software developed in the framework of this project is designed

to implement the most commonly used models available in the literature. In addition, the simulations can be performed with any of these models specified by the user, and the type of simulation can be chosen either coverage study or link study. Depending on the type of services, the study files generated by the simulation of the propagation model are processed to find coverage or interference areas, to calculate link availability, to complete frequency planning and assignment procedures, and to guide international coordination with neighboring countries. All these operations require the integration of various databases into the software. In addition, commercial GIS software have very versatile visualization capabilities, so that it is deemed to be necessary to integrate the software with a commercial GIS to be able to display the simulation results together with the maps and any other spatial data such as roads, boundaries etc. The GIS integrated in the software is the TNT of MicroImages Inc. of Lincoln, Nebraska. One of the selection criteria for choosing the particular GIS was the ability of calling its library functions in our native language (C, C++) codes without using any special programming tools. Two sample outputs of the GIS visualization are shown in Figures 6 and 7. In Figure 6, the coverage area of an analog TV transmitter in Istanbul is shown on the map background. One can directly determine the size of the coverage area and other useful data such as the population inside the coverage contour directly using the library functions of the GIS. Figure 7 shows the useful signal levels and the 95% coverage probability contour for a case study of single frequency network (SFN) of digital video broadcast (DVB-T) in a relatively flat terrain of Turkey.



Fig. 6. 70 dB (uV/m) coverage contour of Çamlıca, Istanbul (N 41° 01' 40", E 29° 04' 08") analog TV station at UHF band with 40 dBW effective radiated power.

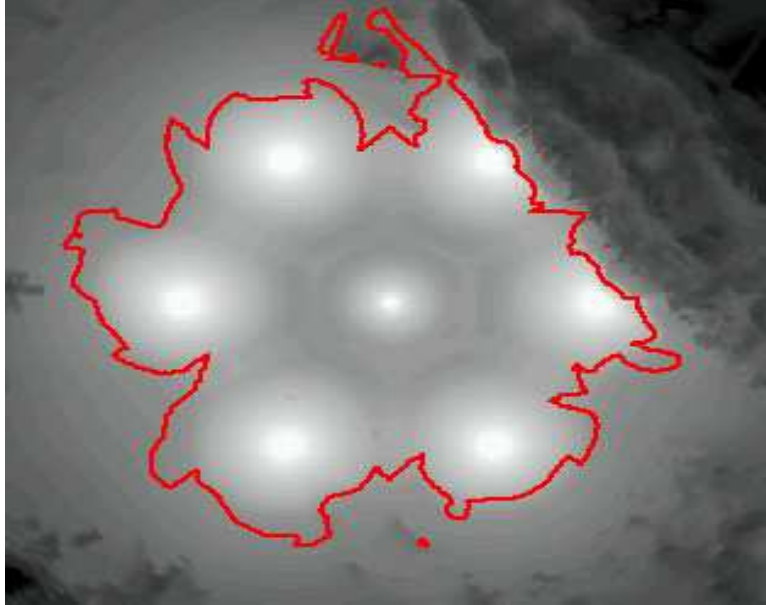


Fig. 7. 95 percent coverage probability contour for a 7-station DVB-T cell structure. The center station is at N 38° 30' 00", E 33° 30' 00". The stations are separated by 27 km., and the central station radiates 100 W, the remaining six stations on the edge of the cell radiate 1 kW each. Frequency is 826 MHz.

5. Conclusions

A propagation prediction software has been developed. The system was integrated with various databases and a GIS. Through the use of real terrain data, various propagation loss models were implemented and compared.

References

1. ITU-R Recommendation P.370-7, "VHF and UHF propagation curves for the frequency range from 30 MHz to 1000 MHz," 1995.
2. ITU-R Recommendation P.526-5, "Propagation by diffraction," 1997.
3. Epstein, J. and Peterson, D. W., "An experimental study of wave propagation at 850 MC," *Proc. Inst. Radio Eng.*, Vol. 41, pp. 595-611, 1955.
4. Deygout, J., "Multiple knife-edge diffraction of radio waves," *IEEE Trans. Antenna Propagat.*, Vol. AP-14, pp. 480-489, April 1966.
5. Deygout, J., "Correction factor for multiple knife-edge diffraction," *IEEE Trans. Antenna Propagat.*, Vol. AP-39, pp. 1256-1258, Aug. 1991.
6. Vogler, L. E., "An attenuation function for multiple knife-edge diffraction," *Radio Science*,

Vol. 17, pp. 1541-1546, Nov.-Dec. 1982.

7. Okumura, Y., Ohmori, E., Kawano, T., and Fukuda, K., "Field strength and its variability in VHF and UHF land mobile radio service," *Review of Electrical Communication Laboratory*, Vol. 16, pp. 825-873, Sept.-Oct. 1968.
8. Hata, M., "Empirical formula for propagation loss in land mobile radio services," *IEEE Trans. Vehicular Tech.*, Vol. VT-29, pp. 317-325, Aug. 1980.
9. ITU-R Recommendation P.1146, "The prediction of field strength for land mobile and terrestrial broadcasting services in the frequency range from 1 to 3 GHz," 1995
10. Walfish, J., and Bertoni, H. L., "A theoretical model of UHF propagation in urban environments," *IEEE Trans. Antenna Propagat.*, Vol. AP-36, pp. 1788-1796, Oct. 1988.
11. Ikegami, F., Yoshida, S., Takeuchi, T., and Umehina, M., "Propagation factors controlling mean field strength on urban streets," *IEEE Trans. Antenna Propagat.*, Vol. AP-32, pp. 822-829, 1984.
12. COST 231 Final Report, "Digital Mobile Radio: COST 231 view on the evolution towards 3rd generation systems," *Commission of the European Communities and COST Telecommunications*, Brussels 1999.
13. S.E. Koonin and D.C. Meredith, *Computational Physics. Fortran Version*, Addison-Wesley, new York, 1990, p.639.
14. T. Anada, T. Fujii, K. Morita, T. Tsuchiya, and N. Endoh, "Numerical Analysis of Long Range Acoustic Propagation Based on Wide Angle Parabolic Wave Equation", *Jap. J. Appl. Phys.*, Vol. 36, Part 1, No. 5B, PP. 3336-3339, May 1997.
15. S. W. Marcus, "A Hybrid (Finite Difference – Surface Green's Function) Method for Computing Transmission Losses in an Inhomogeneous Atmosphere over Irregular Terrain", *IEEE Trans. Antennas and Propagation*, Vol. AP-40, No. 12, PP. 1451-1458, December 1992.
16. M. F. Levy, "Horizontal Parabolic Equation Solution of Radiowave Propagation Problems on Large Domains", *IEEE Trans. Antennas and Propagation*, Vol. AP-43, No. 2, PP. 137-144, February 1995.
17. A. E. Barrios, "A Terrain Parabolic Equation Model for Propagation in the Troposphere", *IEEE Trans. Antennas and Propagation*, Vol. AP-42, No. 1, PP. 90-98, January 1994.